Urchin-like Ce/Tb co-doped GdPO4 hollow spheres for in vivo luminescence/X-ray bioimaging and drug delivery

Journal:	*Biomaterials Science*
Manuscript ID:	BM-ART-05-2014-000158.R1
Article Type:	Paper
Date Submitted by the Author:	09-Jun-2014

Complete List of Authors:	Yi, Zhigao; Faculty of Material & Photoelectronic Physics, Xiangtan University lu, wei; Faculty of Applied Science and Textiles The Hong Kong Polytechnic University, Department of Applied Physics Qian, Chao; College of Physics and Information Science,Hunan Normal University, Zeng, Tianmei; College of Physics and Information Science, Hunan Normal University Yin, Lingzhen; College of Physics and Information Science,Hunan Normal University, Wang, Haibo; Faculty of Material & Photoelectronic Physics, Xiangtan University Rao, Ling; Faculty of Material & Photoelectronic Physics, Xiangtan University Liu, Hongrong; College of Physics and Information Science, Hunan Normal University zeng, songjun; College of Physics and Information Science , Hunan Normal University;

Journal Name

Dynamic Article Links ►

Cite this: DOI: 10.1039/c0xx00000x

www.rsc.org/xxxxxx

ARTICLE TYPE

Urchin-like Ce/Tb co-doped $GdPO_4$ hollow spheres for *in vivo* luminescence/*X-ray* bioimaging and drug delivery

Zhigao Yi, [a,b] Wei Lu, [c] Chao Qian, [a] Tianmei Zeng, [a] Lingzhen Yin, [a] Haibo Wang, [a,b] Ling Rao, [a,b] Hongrong Liu, [a] Songjun Zeng [*,a]

Received (in XXX, XXX) Xth XXXXXXXXX 20XX, Accepted Xth XXXXXXXXX 20XX

DOI: 10.1039/b000000x

In this paper, we report a self-sacrificing route for fabrication the Ce/Tb co-doped $GdPO_4$ hollow spheres in the hydrothermal condition using the $Gd(OH)CO_3$:Ce/Tb precursor as template and $NH_4H_2PO_4$ as phosphorus source. The X-ray diffraction (XRD) patterns show the amorphous crystal nature of the precursor and pure hexagonal phase of the hollow spheres. The microstructure of the as-prepared precursor and hollow spheres were characterized by transmission electron microscopy (TEM) and scanning TEM (STEM) assays. The results exhibit urchin-like morphology of the solid precursor and hollow spheres. Bright green emissions of the spheres have been detected using an ultraviolet (UV) lamp at 288 nm and the calculated CIE coordinates are (0.289, 0.491). The energy transfer mechanism of Ce and Tb ions in $GdPO_4$ host has been investigated. The quantum efficiency of the hollow spheres was measured to 61% and the lifetime calculated as 6.94 ms. In addition, the magnetic mass susceptibilities and magnetization of the spheres are found to be 6.39×10^{-5} emu/gOe and 1.27 emu g^{-1} at 20 kOe, respectively. Owing to the excellent downshift luminescence property, the as-prepared $GdPO_4$:Ce/Tb hollow spheres have been successfully applied in *in vivo* luminescence and X-ray bioimaging for the first time. Moreover, the three-dimensional (3D) *in vivo* X-ray bioimaging of the mouse can provide the accurate location from multiple directions. The high-contrast ratio makes the spheres a promising X-ray contrast agent. Due to the hollow structure, these $GdPO_4$:Ce/Tb hollow spheres were also used as drug delivery system for doxorubicin (DOX) loading and releasing. The drug loading efficiency is measured to 17% at pH value of 7.4, and the pH-dependent drug release was studied. 47% of the loaded DOX was released within 10 h when pH =5, while there was only 30% in the same time at pH = 7.4 and it took nearly 48 h to reach a comparable level. The different release nature makes these spheres a promising application in targeting therapy of tumor.

1. Introduction

Hollow nano-/micro-materials with controllable size and morphology have attracted increasing research interest in modern chemistry and materials research areas, owing to their outstanding properties, such as, lower density, larger specific area, encapsulation ability and surface permeability.[1-6] Therefore, these hollow structural materials have promising applications in various fields such as biotechnology, drug delivery, catalysis, fillers, photonic devices, electrochemical cells, and waste removal.[7-14] With the development of these functional materials, a variety of fabricated methods have been exploited. However, among the various strategies, template route is the most usual and efficient way to obtain hollow structures. Of course, whether on the basis of hard templates (consisting of polystyrene, silica particles and carbon spheres)[15-21] or building on soft templates (including supramolecules, surfactants and polymer vesicles),[22-26] all of these strategies have exhibited some shortcomings. According to the former method, a large amount of time is necessary due to the multistep fabrication and removal of the templates. While, there is a huge challenge of controlling the shape and size of the final products through the latter. In addition, hollow spherical nanocrystals can also be obtained by template free routes[27] which make use of the mechanism of the Ostwald ripening process. In comparison to the methods mentioned above, the template route of self-sacrificing gathers their advantages and can receive ideal morphology simultaneously.[28-30]

Recently, many works have been focused on synthesizing hollow spherical rare-earth (RE) compounds.[31-41] For instance, as reported,[33] Gd_2O_3 hollow microspheres with uniform morphology and well dispersity have been successfully synthesized using self-sacrificing method and lanthanide ions (Ln^{3+}) doped Gd_2O_3 microspheres show excellent luminescence capacities. In addition, Gd_2O_3 hollow spheres were fabricated by homogeneous precipitation method where carbon spheres were utilized as templates and removed by calcination. The as-prepared spheres have been applied as positive T_1 contrast agents for magnetic resonance imaging and drug delivery host carriers for studying

the drug loading/release properties of these hollow structure spheres as well as their promising therapeutic application. Besides, Gd^{3+}-based hosts can also act as ideal candidates of contrast agents for X-ray imaging because of the huge K-edge values ($Gd_{K\text{-}edge}$ = 50.2 keV) and the large X-ray absorption efficiency of the Gd element (at 80 keV, Gd = 5.57 cm^2 g^{-1}).[42-44] Therefore, much more efforts have been made to exploit new system of Gd^{3+}-based host in conjugation with the hollow structure. As represented, $GdVO_4$:Dy microspheres,[37] GdF_3 micro/nano-spheres,[40] and Gd_2O_2S:Tb nanocapsules[41] have been fabricated and exhibited their unique microstructural and luminescent properties and application in bioimaging and drug loading/release capabilities. Very recently, Eu^{3+} doped $GdPO_4$ hollow spheres come into our sight, but the workers have just showed their fluorescent and paramagnetic nature.[30,46] However, integration of *in vivo* bioimaging and drug delivery in a system of Ln^{3+} doped $GdPO_4$ hollow spheres have not been exploited. In addition, previous literatures proved the high efficiency of energy transfer between Ce and Tb in phosphors, which inspired us to dope Ce and Tb into $GdPO_4$ host for intense emissions and further bioimaging.

In this paper, Ce/Tb co-doped $GdPO_4$ spheres with urchin-like hollow structure were fabricated using a typical self-sacrificing route with some modification. The crystal phase and microstructure of the precursor (Carbonate hydroxide gadolinium, $Gd(OH)CO_3$) and final products were studied firstly. Then, the downshift luminescence and paramagnetic properties of the as-prepared spheres were studied in detail. Furthermore, these as-prepared spheres were at the first time used for *in vivo* luminescence, X-ray, 3D X-ray bioimaging, and drug loading/release investigation. The results indicate that the obtained Ce/Tb co-doped $GdPO_4$ hollow spheres may be a new generation of biolabels, contrast agents, drug delivery carriers and therapeutic agents.

2. Experimental

2.1 Chemicals and materials

The RE oxides Gd_2O_3, Ce_2O_3, and Tb_2O_3 are all of 99.99% purity and were purchased from Sigma-Aldrich. The corresponding RE nitrides $RE(NO_3)_3$ were obtained via dissolving oxides into dilute nitric acid under heating with sequential stirring until the formation of transparent solution. Evaporate the remaining solvent and prepare the final solution with a designed concentration of 0.5 M. The other chemicals (analytical grade) were bought from Sinopharm Chemical Reagent Co., China. All of these reagents were used with no further purification.

2.2 Synthesis of the $Gd(OH)CO_3$: Ce/Tb Precursor

The urchin-like colloidal $Gd(OH)CO_3$:Ce/Tb precursor with monodispersity were prepared by a modified homogeneous precipitation method utilizing urea [$CO(NH_2)_2$] as precipitator.[47] In a typical synthesis, the as-prepared $Gd(NO_3)_3$, $Ce(NO_3)_3$, and $Tb(NO_3)_3$ solution with a total amount of 1 mmol and designed molar ratio of 75:20:5 were dissolved into 50 mL deionized (DI) water. 2.0 g of urea was then added into the former mixture with vigorously stirring. The solution was further stirring for another 2 h at room temperature. The obtained solution was then heated to 80 °C and maintained for 2 h in the oil bath. After the reaction accomplished completely, the milky-white suspension was separated and collected by centrifugation. The impurities were washed with ethanol and DI water three times. The obtained precursor was dispersed into 20 mL of DI water for further use.

2.3 Synthesis of the $GdPO_4$:Ce/Tb Hollow Spheres

In a typical synthesis, the as-prepared $Gd(OH)CO_3$:Ce/Tb water solution was labeled as solution A after ultrasonication for 30 min. 0.115 g of $NH_4H_2PO_4$ and 0.1 g of cetyltrimethyl ammonium bromide (CTAB) were added into 20 mL of DI water under stirring to form homogeneous solution B. Solutions A and B were then mixed together with vigorous agitation. Finally, 40 mL of the resultant mixture was transferred into a 50 mL stainless steel autoclave. The system was sealed and maintained at 200 °C for 15 h. After the reaction, the products were cooled to room temperature naturally and the final products were assembled in the bottom of the vessel. The supernatant solution was poured directly and the precipitates were separated and collected via centrifugation. The impurities were removed by washing with ethanol and DI water in sequence. The as-prepared $GdPO_4$:Ce/Tb hollow spheres were dried in air at 60 °C for 24 h.

2.4 Characterization

The crystal phase of the $Gd(OH)CO_3$:Ce/Tb precursor and the $GdPO_4$:Ce/Tb spheres were recorded by powder XRD using a D/max-γA system X-ray diffractometer at 40 kV and 250 mA with Cu-Kα radiation (λ = 1.54056 Å). The shape and size of these as-synthesized samples were observed using TEM and STEM (JEOL-2100F). Secondary electron image (SEI) at STEM mode was acquired. During the TEM assay, the composed elements of the spheres were detected via the energy-dispersive X-ray spectrum (EDS) affiliated to the TEM. The surface ligands of the samples were detected through Fourier transform infrared spectrum (FTIR) employing a Magna 760 spectrometer (Nicolet). The luminescence spectra of the samples were recorded by a Zolix Analytical Instrument (fluoroSENS 9000A) equipped with a Xe lamp (400W) at room temperature. After the luminescence assays, the luminescence decay curve of the $GdPO_4$:Ce/Tb spheres was tested (major parameters: λex = 288 nm, λem = 543 nm, excitation/emission bandpass: 8 mm, and integrate time: 100 μs) The digital photograph of the water solution containing 1 wt% of the spheres was taken by a Canon digital camera under the excitation of a UV lamp at 253 nm in the dark. The magnetic property of the as-prepared $GdPO_4$:Ce/Tb spheres was detected via a vibrating sample magnetometer (VSM, Lake-shore 7410) and the applied field was ranged from -20 to 20 kOe.

2.5 *In vivo* Luminescence Bioimaging

For the purpose of measuring the feasibility of the *in vivo* luminescence bioimaging based on the $GdPO_4$:Ce/Tb spheres, a Kunming mouse was firstly anesthetized via intraperitoneal injection of 100 μL 10 wt% pentobarbital sodium water solution. Then, the mouse was subcutaneously injected 200 μL of the

$GdPO_4$:Ce/Tb aqueous solution (2 mg/mL). After injection, *in vivo* luminescence bioimaging was observed through an *in vivo* imaging system (Bruker In-Vivo FX PRO). The luminescence bioimaging was captured under the excitation of 470 nm using a band pass filter (600/40 nm) with exposure time of 5 s. All animal procedures comply with the institutional animal use and care regulations, approved by the Laboratory Animal Center of Hunan.

2.6 *In vivo* X-ray Bioimaging

To demonstrate the X-ray bioimaging based on these $GdPO_4$:Ce/Tb spheres, the *in vivo* X-ray bioimaging was carried out. Then, another mouse was subcutaneously injected 200 μL of the $GdPO_4$:Ce/Tb aqueous solution (2 mg/mL) for the X-ray bioimaging at different sites. The X-ray bioimaging was also detected by the *in vivo* imaging system equipped with an X-ray imaging functionality with an operating voltage of 0-45 kVp. The X-ray bioimaging was recorded under the operating voltage of 45 kVp (filter = 0.8 mm and exposure time = 1 min). The 3D X-ray bioimaging was captured by the multimodal animal rotation system (MARS, per 10° ranging from 0 to 360°) and the images were exported as a video at 5 frames per second.

2.7 *In Vitro* Drug Loading and Release

To measure the drug loading capabilities of the $GdPO_4$:Ce/Tb hollow spheres, DOX (Shanghai Ekear Bio&Tech Co., Ltd) loading into the hollow spheres was done by adding 0.5 mg of these powders into 2 mL and 0.1 mg/mL of DOX phosphate buffer solution (PBS, pH = 7.4). The suspension was shaken for 24 h at room temperature for achieving the equilibrium state. The solution was then centrifuged at 12000 rpm for 10 min to collect the DOX-loaded spheres and remove the free DOX. The supernatant was retained and the concentration of DOX loaded on the hollow spheres was measured via the DOX characteristic absorption peak at 480 nm after subtracting the absorbance ascribed to the hollow spheres at the same wavelength.[48,49] The UV-vis absorbance spectra were detected using a Lambda 750 UV/VIS spectrometer (PerkinElmer Inc.).

To investigate the DOX release kinetics, the obtained DOX loaded $GdPO_4$:Ce/Tb hollow spheres were incubated in PBS with two pH values (5 and 7.4) and soaked all the time. At the designed time interval, DOX released from the hollow spheres was collected by centrifugation and the amounts of released DOX in the supernatant were recorded by the UV-vis absorbance spectrum. All the measurements were done for three times and then took the average value.

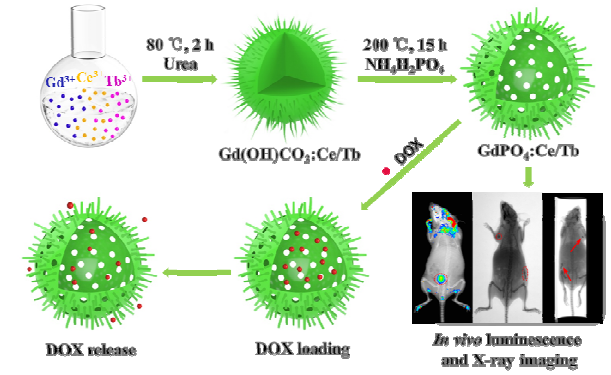

Scheme 1. Scheme for the preparation process of $GdPO_4$:Ce/Tb hollow spheres, *in vivo* luminescence and X-ray bioimaging, and drug loading/release.

3. Results and Discussion

3.1 Structure Characterization

As demonstrated in Scheme 1, The urchin-like $Gd(OH)CO_3$:Ce/Tb precursor was obtained by homogeneous precipitation method using urea as precipitator. Then, the urchin-like $GdPO_4$:Ce/Tb hollow spheres were prepared via self-sacrificing template route in which the precursor interacted with the added $NH_4H_2PO_4$ under hydrothermal conditions. The as-prepared spheres have successfully applied in *in vivo* fluorescence, X-ray and 3D X-ray bioimaging. Moreover, the hollow structure of these spheres shows its excellent drug loading and release capabilities.

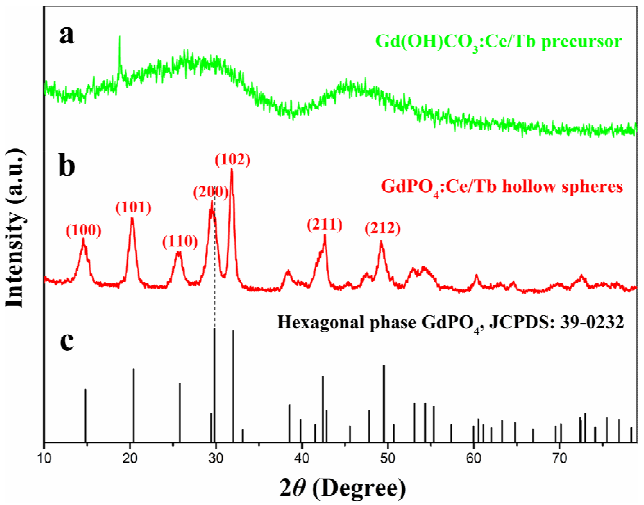

Figure 1. XRD patterns of (a) $Gd(OH)CO_3$:Ce/Tb, (b)$GdPO_4$:Ce/Tb, and (c) JCPDS card of the pure hexagonal phase $GdPO_4$.

The crystal phases of the as-prepared samples were first recorded by XRD. Figure 1 shows the XRD results of the $Gd(OH)CO_3$:Ce/Tb precursor and $GdPO_4$:Ce/Tb hollow spheres. As shown in Figure 1a, the XRD pattern of the precursor exhibits board bands ranging from 15° to 60° indicating the amorphous structure of these precursor.[50] The diffraction peaks of $GdPO_4$:Ce/Tb hollow spheres (Figure 1b) were well indexed to the pure hexagonal phase $GdPO_4$ crystal and the relative diffraction intensities of these peaks were mainly coincident with the data cited from the Joint Committee on Powder Diffraction

Standards (JCPDS, number 39-0232). The slightly shifting towards lower angle side of the diffraction peak is ascribed to the enlarged unit-cell volume of $GdPO_4$ matrix for the replacement of Gd^{3+} (r = 1.193 Å) by Ce^{3+} with relatively larger radius (r = 1.283 Å).[51] Moreover, no other peaks of impurity were detected from the XRD pattern which implied the formation of the pure hexagonal phase $GdPO_4$:Ce/Tb.

The shape and size of the as-prepared precursor and final products were characterized by TEM analysis. As shown in panels a and b in Figure 2, typical TEM reveal that the nearly spherical and prickly structures of the both. In addition, SEI acquired at STEM mode (Figure 2c and e) demonstrated that the surface of the precursor was made up by the nanowires and the external of $GdPO_4$:Ce/Tb was composed of nanorods. In comparison with the high-magnification TEM images of these two species, the internal of the precursor shows solid state and the final products are hollow, respectively (Figure 2d and f). Of course, these changes of morphology should be contributed to the hydrothermal process via adding $NH_4H_2PO_4$. Figure 2g demonstrates the elemental composition of the $GdPO_4$:Ce/Tb hollow spheres, indicating the presence of Gd, P, O, Ce, and Tb. Note that the detected Cu and C signals originate from the the Cu grid of TEM sample.

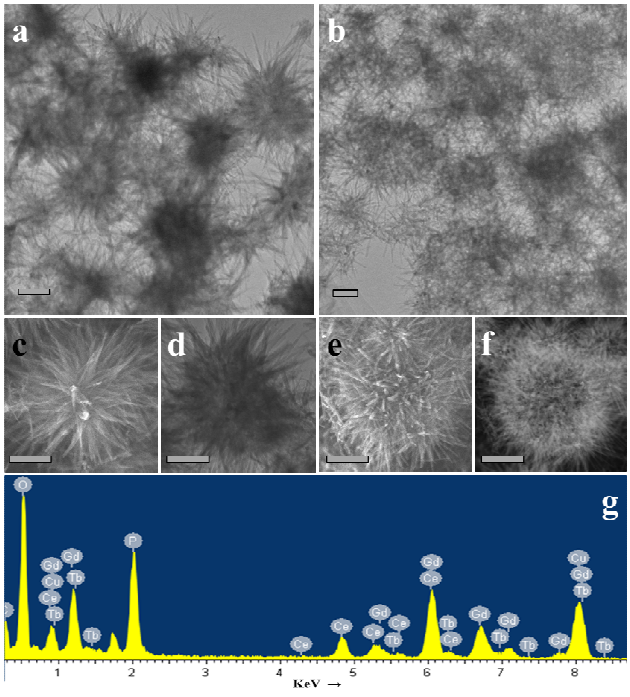

Figure 2. Morphology and microstructure study: (a) and (b) typical TEM images, (c) and (e) SEI images, and (d) and (f) high-magnification TEM images of $Gd(OH)CO_3$:Ce/Tb and $GdPO_4$:Ce/Tb, respectively; (g) EDS of a sphere in e. The scale bars are all 200 nm for a-f.

3.2 FTIR analysis

As shown in Figure 3, the surface functional groups of the precursor and hollow spheres were identified by FTIR spectra. As demonstrated in Figure 3a, the characteristic peaks at 3393, 1506, 1410, 1077, 843, and 742 cm^{-1} are ascribed to OH (υ), CO (υ_{as}), CO (υ_{as}), CO (υ_s), CO (δ), and OH (δ), where the υ, υ_{as}, υ_s, and δ stand for stretch, asymmetric stretch, symmetric stretch, and deformation, respectively, implying that the composition of the precursor should be $Gd(OH)CO_3$.[35,39] However, the absorption bands at 620 and 543 cm^{-1} and a broad band at 1067 cm^{-1} reveal the presence of phosphate groups (Figure 3b).

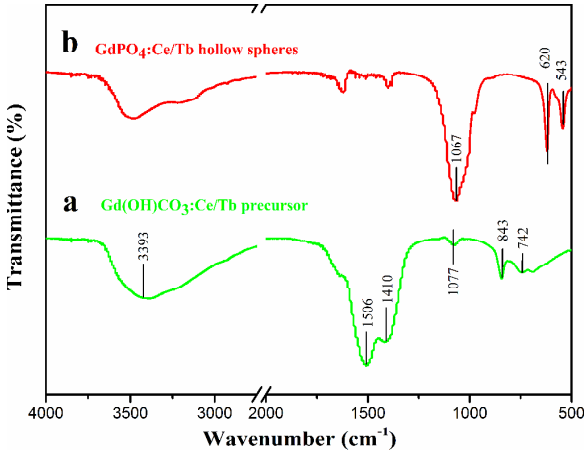

Figure 3. The FTIR spectra of (a) the $Gd(OH)CO_3$:Ce/Tb precursor and (b) the $GdPO_4$:Ce/Tb hollow spheres.

3.3 Photoluminescence (PL) and magnetization properties

The luminescence of Ce/Tb co-doped phosphors and the energy transfer from Ce to Tb ions have been well investigated by previous works.[52,53] As demonstrated in Figure 4, the energy transfer firstly occurred between Ce^{3+} and Ce^{3+} under the UV irradiation at 288 nm. Then, the energy transferred from Ce^{3+} (5d) to Tb^{3+} ($4f^9$), followed closely by the cross relaxation the Tb^{3+} ($^5D_4$). The $^5D_4$ levels of Tb^{3+} radioactively transferred to the lower energy levels of ^7F_J (J = 0, 1, 2, 3, 4, 5, 6). Owing to the high efficiency of these energy transfer in Ce/Tb co-doped $GdPO_4$ host, as the inset shown in Figure 5, the digital photograph of the water solution containing 1 wt% $GdPO_4$:Ce/Tb spheres exhibits intense eye-visible green light under the excitation of a 253 nm UV lamp in the dark at room temperature. Figure 5 exhibits the excitation and emission spectra of these hollow spheres. The excitation spectrum (green curve) shows a week band centered at 222 nm and a high and broad band ranging from 250 to 350 nm with a maximum at 288 nm. The former attribute to the $4f^8$-$4f^7$5d transitions of Tb^{3+} and the latter are ascribed to the 5d-4f transition of Ce^{3+}. The bright and strong emissions of Tb^{3+} (488 nm: $^5D_4$-$^7F_6$, the strongest 543 nm: $^5D_4$-$^7F_5$, 587 nm: $^5D_4$-$^7F_4$, and 596 nm: $^5D_4$-$^7F_3$) are yielded under excitation of 288 nm. A further color coordinates calculation reveals that the luminescence of the $GdPO_4$:Ce/Tb hollow spheres located in the region of green in Commission Internationale de I'Eclairage 1931 chromaticity (CIE 1931) and the calculated coordinates are (0.289, 0.491). In addition, the quantum yield of the $GdPO_4$:Ce/Tb spheres was measured to 61%, further implying energy transfer from Ce^{3+} to Tb^{3+} in $GdPO_4$ host.

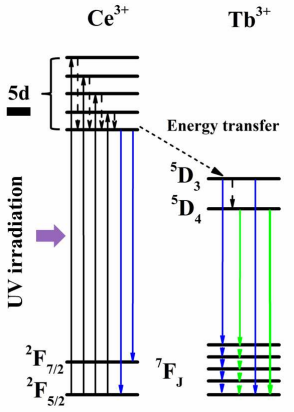

Figure 4. Energy transfer mechanism and downshift luminescence emission of the $GdPO_4$:Ce/Tb hollow spheres under the excitation of a UV lamp at 288 nm.

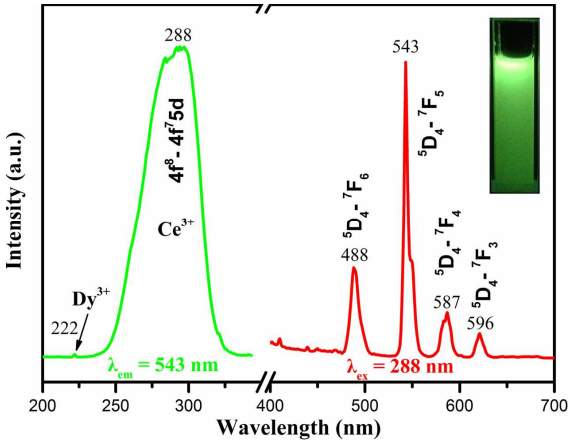

Figure 5. Excitation and emission spectra of the $GdPO_4$:Ce/Tb hollow spheres, Inset is the digital photograph of aqueous solution (1 wt%) under the 253 nm UV lamp irradiation in a sealed room.

Moreover, the decay curve of the as-prepared spheres has been detected. As shown in Figure 6, the square dots represent the experimental data and the red solid line indicates the fitting result. The luminescence lifetime can be estimated by the following formula $I(t) = I_0\exp(-t/\tau)$, where τ stands for the lifetime of the emitted lanthanide ions. The lifetime shown by the fitting result via the formula is 6.94 ms.

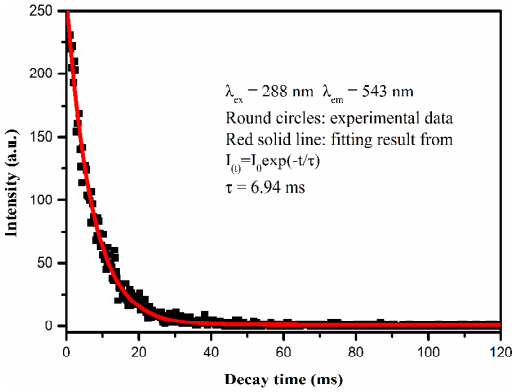

Figure 6. Decay curve of $GdPO_4$:Ce/Tb hollow spheres.

In addition to the excellent luminescence properties, the $GdPO_4$:Ce/Tb hollow spheres also possess attractive paramagnetic nature which is ascribed to the large magnetic moment of Gd^{3+} (7.94 μ_B)[50] in $GdPO_4$ host. Figure 7 shows the magnetization of the $GdPO_4$:Ce/Tb hollow spheres as a function of applied field ranging from -20 to 20 kOe at room temperature. As demonstrated, these $GdPO_4$:Ce/Tb hollow spheres present paramagnetic property at room temperature. The paramagnetic behavior of the $GdPO_4$:Ce/Tb hollow spheres is primarily ascribed to the seven unpaired inner 4f electrons, which are closely bound to the nucleus and effectively shielded by the outer closed shell electrons from the crystal field.[42-45] The magnetic mass susceptibility and magnetization of the $GdPO_4$:Ce/Tb hollow spheres are at ~ 6.39×10^{-5} emu/gOe and ~ 1.27 emu/g at 20 kOe, respectively. The results indicate that the $GdPO_4$:Ce/Tb hollow spheres can act as contrast agents for magnetic resonance imaging.

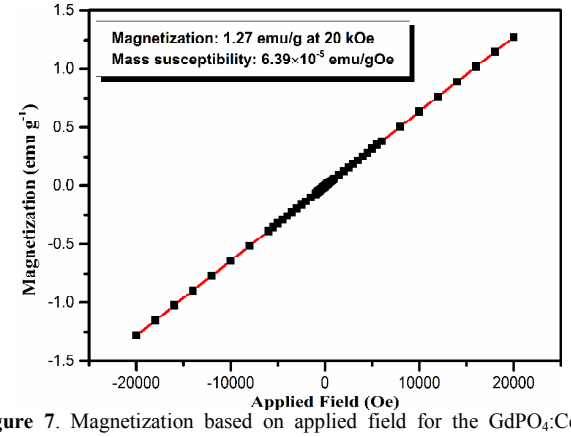

Figure 7. Magnetization based on applied field for the $GdPO_4$:Ce/Tb hollow spheres at room temperature.

3.4 *In Vivo* Luminescence Bioimaging

The toxicity and biocompatibility of the hollow spheres in the same $GdPO_4$ host lattice have been studied by previous work,[39] in which the $GdPO_4$:Eu spheres show well biocompatibility and have been proved as non-toxic materials for biomedical applications. To measure the feasibility of the $GdPO_4$:Ce/Tb hollow spheres for *in vivo* luminescence bioimaging, a Kunming mouse was subcutaneously injected with 200 μL of the aqueous solution of $GdPO_4$:Ce/Tb hollow spheres (2 mg/mL). After 5 min injection, the mouse was observed for *in vivo* luminescence bioimaging using a multi-modal *in vivo* imaging system (Bruker In-Vivo FX PRO) under the excitation of a 400 W Xenon lamp at 470 nm. Figure 8a and 8b show the *in vivo* whole-body images of the mouse without and with subcutaneous injection of the $GdPO_4$:Ce/Tb hollow spheres, respectively. The high-contrast luminescence signal in the mouse injected with spheres was observed (labeled by red-dotted circles). Figure 8c shows the overlay image, where the luminescence signals are matched well with the whole body of the mouse. Of course, the autofluorescence of the mouse and the lower penetration of UV wavelengths are inevitable shortcomings, limiting the application in *in vivo* whole-body luminescence bioimaging of these downshifting nanocrystals.

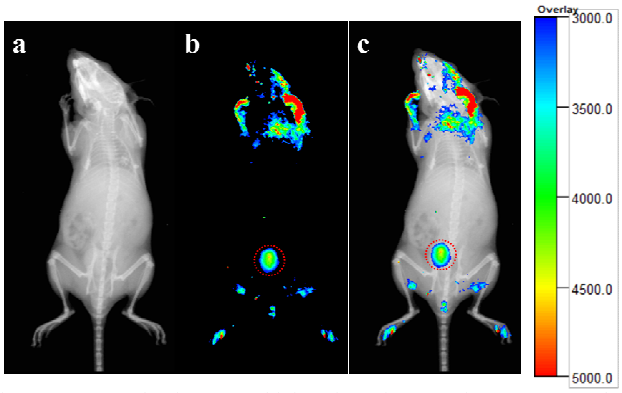

Figure 8. *In vivo* luminescence bioimaging of a Kunming mouse: (a) the X-ray image before injection, (b) the luminescence image after injecting the as-prepared spheres, (c) the overlay of a and b.

3.5 *In Vivo* X-ray Bioimaging

Apart from *in vivo* luminescence bioimaging, the $GdPO_4$:Ce/Tb hollow spheres can be used as X-ray bioimaging contrast agents due to the large K-edge values and X-ray absorption coefficient of the Gd element. To reveal the *in vivo* X-ray bioimaging of these spheres, a Kunming mouse was subcutaneously injected with PBS containing these spheres. After 5 min injection, *in vivo* X-ray bioimaging was performed using a multifunctional *in vivo* imaging system under voltage of 45 kVp. Figure 9 shows the *in vivo* X-ray bioimaging in a Kunming mouse. As observed in Figure 9a, there are no X-ray signals detected in the untreated mouse. The high-contrast X-ray absorption contrasts indicated by the red-dotted circles (Figure 9b) are observed after subcutaneous injection with spheres. Moreover, The 3D *in vivo* X-ray bioimaging of the mouse (in the supporting information, **Movie S1**) was captured using the protocol model in the multifunctional *in vivo* imaging system and an image of which is shown in Figure 3c. These 3D X-ray bioimaging can demonstrate the accurate location of the spheres from multiple directions and have a promising application in clinic treatment.

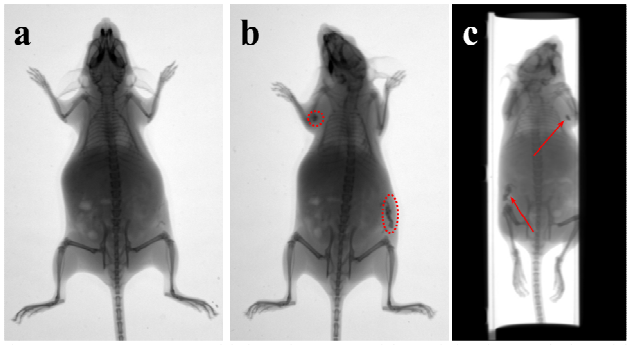

Figure 9. *In vivo* X-ray bioimaging: (a) without injection and (b) with subcutaneous injection with the as-prepared spheres in two regions of a Kunming mouse, (c) an image of the 3D *in vivo* X-ray bioimaging.

3.6 Drug Loading and Release

Owing to the hollow structure of the spheres, efforts have been made to utilizing the as-prepared hollow spheres as drug host carriers. As demonstrated by former FTIR result, large amounts of hydroxyl groups are on the surface of the $GdPO_4$:Ce/Tb hollow spheres after hydrothermal reaction. Therefore, the obtained spheres with negative charges of hydroxyl groups can easily interact with the positively charged DOX molecules with protonated primary amine group in a neutral condition. Thus, the electrostatic interaction aforementioned provides the main driving force for DOX loading. In addition, the size distribution of the as-prepared hollow spheres in PBS (0.25 mg/mL) was tested by dynamic light scattering. As shown in Figure S1, the diameter of the spheres was measured to be 865.6 ± 40.25 nm. To qualitatively study the loading efficiency of DOX, the solution containing the spheres and DOX with designed molar ratio was measured by centrifugation and then sonication. As shown in left panel of Figure 10a, in comparison with the free DOX, the mixture of the spheres and DOX exhibits a weaker red color. In addition, reddish precipitate and nearly transparent liquid were observed after centrifugation indicating the binding of DOX on the spheres. As a comparison in upper panel of figure 10a, the free DOX shows no obvious color change and precipitate. The latter quantified assay of DOX loading efficiency is based on UV-vis spectra according to the characteristic adsorption peak of DOX at 480 nm, due to the linear relation between the amounts of DOX and the intensity of adsorption peak at 480 nm.[37,39] The DOX loading efficiency of the spheres was calculated to 17%.

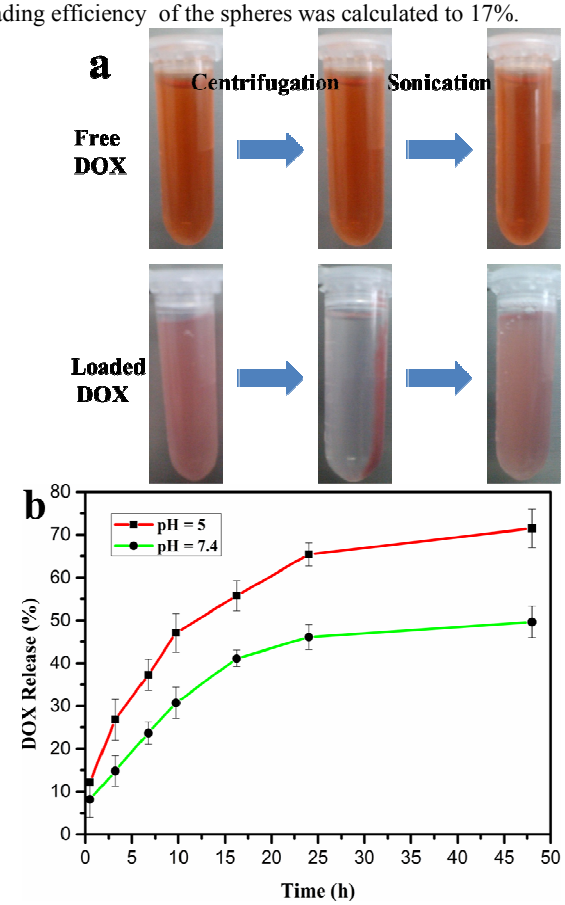

Figure 10. Preparation and characterization of the DOX-loaded spheres: (a) photographs of free DOX and DOX-loaded spheres after centrifugation and sonication, (b) UV-vis absorbance spectra of free DOX, and (c) DOX release from the spheres over time in PBS at pH = 5 and 7.4. Error bars are standard deviations based on triplicated samples.

The accumulated DOX release of the DOX-loaded

$GdPO_4$:Ce/Tb hollow spheres were detected in PBS with two pH values (5 and 7.4). As shown in Figure 10c, at pH = 5, 47% of the loaded DOX was released within 10 h, whereas at pH = 7.4, there was only 30% in the same time and it took nearly 48 h to reach a comparable level (47%). In addition, to assess the stability of the particles, the solution of these particles after drug release was used for FE-SEM analysis (shown in Figure S2). It can be seen that the particles are still urchin-like and the structure is maintained without any damage. The electrostatic interaction aforementioned is weaker in acidic condition than that in neutral which is the major factor of rapid release at pH=5. These different release nature indicates that the release rate of physically bounded DOX is faster in tumor areas (mild acidic conditions) than that in the blood (neutral environments),[37] which makes the DOX-loaded hollow spheres a promising application in targeting therapy of tumor.

4. Conclusion

In summary, the hexagonal phase Ce/Tb co-doped $GdPO_4$ spheres with urchin-like hollow structure have been fabricated by self-sacrificing route. The obtained spheres exhibit bright green emissions under the excitation of 288 nm and paramagnetic properties (the magnetic mass susceptibility: 6.39×10^{-5} emu/gOe and magnetization: 1.27 emu/g at 20 kOe). The as-prepared spheres have been successfully applied in *in vivo* luminescence, X-ray, and 3D X-ray bioimaging. The loading efficiency are measured to 17% at pH = 7.4 and the release ratio was calculated to 47% within 10 h (pH = 5). The excellent drug loading and release capabilities make the hollow spheres ideal candidate for targeted therapy.

Acknowledgments

This work was supported by the National Natural Science Foundation of China (Nos. 51102202, and 31370736), Specialized Research Fund for the Doctoral Program of Higher Education of China (No. 20114301120006) and Hunan Provincial Natural Science Foundation of China (No. 12JJ4056), and Scientific Research Fund of Hunan Provincial Education Department (13B062).

Notes and references

[a] *College of Physics and Information Science and Key Laboratory of Low-dimensional Quantum Structures and Quantum Control of the Ministry of Education, Hunan Normal University, Changsha, Hunan, People's Republic of China. Email: songjunz@hunnu.edu.cn*

[b] *Faculty of Materials, Optoelectronics and Physics, Key Laboratory of Low-dimensional Materials and Application Technology (Ministry of Education), Xiangtan University, Xiangtan 411105, People's Republic of China.*

[c] *Department of Applied Physics and Materials Research Center, The Hong Kong Polytechnic University, Hong Kong.*

1 Y. Chen, H. R. Chen, L. M. Guo, D. P. Zeng, Y. B. Tian, F. Chen, J. W. Feng and J. L. Shi, *ACS Nano*, 2010, **4**, 6001.

2 G. Jia, M. Yang, Y. H. Song, H. P. You and H. J. Zhang, *Cryst. Growth Des.*, 2009, **9**, 301.

3 Z. X. Wang, L. M. Wu, M. Chen and S. X. Zhou, *J. Am. Chem. Soc.*, 2009, **131**, 11276.

4 X. W. Lou, L. A. Archer and Z. C. Yang, *Adv. Mater.*, 2008, **20**, 3987.

5 K. Cheng and S. H. Sun, Nano Today, 2010, **5**, 183.

6 L. Li, R. Z. Ma, N. Iyi, Y. Ebina, K. Takada and T. Sasaki, *Chem. Commun.*, 2006, **29**, 3215.

7 S. Kidambi, J. H. Dai, J. Li and M. L. Bruening, *J. Am. Chem. Soc.*, 2004, **126**, 2658.

8 Y. Wang, L. Cai and Y. Xia, *Adv. Mater.*, 2005, **17**, 473.

9 Z. Z. Yang, Z. W. Niu, Y. F. Lu, Z. B. Hu and C. C. Han, *Angew. Chem., Int. Ed.*, 2003, **42**, 1943.

10 Y. S. Li, J. L. Shi, Z. L. Hua, H. R. Chen, M. L. Ruan, D. S. Yan, *Nano. Lett.*, 2003, **3**, 609.

11 X. F. Yu, D. S. Wang, Q. Peng and Y. D. Li, *Chem. Commun.*, 2011, **47**, 8094.

12 H. J. Kim, K. II. Choi, A. Q. Pan, II. D. Kim, H. R. Kim, K. M. Kim, C. W. Na, G. Z. Cao and J. H. Lee, *J. Mater. Chem.*, 2011, ***21***, 6549.

13 Y. Q. Wang, G. Z. Wang, H. Q. Wang, C. H. Liang, W. P. Cai and L. D. Zhang, *Chem. Eur. J.*, 2010, ***16***, 3497.

14 Y. F. Zhu, J. L. Shi, W. H. Shen, X. P. Dong, J. W. Feng, M. L. Ruan and Y. S. Li, *Angew. Chem., Int. Ed.*, 2005, ***44***, 5083.

15 Y. G. Sun, B. T. Mayers and Y. N. Xia, Nano Lett., 2002, ***2***, 481.

16 K. J. Son, H. J. Yoon, J. H. Kim, W. D. Jang, Y. Lee and W. G. Koh, *Angew. Chem., Int. Ed.*, 2011, ***50***, 11968.

17 S. Han, K. Sohn and T. Hyeon, Chem. Mater., 2001, ***12***, 3337.

18 S. H. Tang, X. Q. Huang, X. L. Chen and N. F. Zheng, *Adv. Funct. Mater.*, 2010, ***20***, 2442.

19 X. M. Sun and Y. D. Li, *Angew. Chem., Int. Ed.*, 2004, ***43***, 3827.

20 X. M. Sun, J. F. Liu and Y. D. Li, *Chem. Eur. J.*, 2006, ***12***, 2039.

21 H. S. Qian, G. F. Lin, Y. X. Zhang, P. Gunawan and R. Xu, *Nanotechnology*, 2007, ***18***, 355602.

22 D. P. Yang, S. H. Chen, P. Huang, X. S. Wang, W. Q. Jiang, O. Pandoli and D. X. Cui, *Green Chem.*, 2010, ***12***, 2038.

23 Q. Peng, Y. J. Dong, Y. D. Li, Angew. Chem., Int. Ed., 2003, ***42***, 3027.

24 J. Liu, S. B. Hartono, Y. G. Jin, Z. Li, G. Q. Lu and S. Z. Qiao, J. *Mater. Chem.*, 2010, ***20***, 4595.

25 S. S. Feng, Z. Y. Ren, Y. L. Wei, B. J. Jiang, Y. Liu, L. Y. Zhang, W. B. Zhang and H. G. Fu, *Chem. Commun.*, 2010, ***46***, 6276.

26 J. Bao, Y. Liang, Z. Xu and L. Si, *Adv. Mater.*, 2003, **15**, 1832.

27 P. L. Lu, Y. C. Chen, T. W. Ou, H. H. Chen, H. C. Tsai, C. J. Wen, C. L. Lo, S. P. Wey, K. J. Lin, T. C. Yen and G. H. Hsiue, *Biomaterials*, 2011, **32**, 2213.

28 F. Zhang, Y. F. Shi, X. H. Sun, D. Y. Zhao and G. D. Stucky, *Chem. Mater.*, 2009, **21**, 5237.

29 Y. D. Yin, R. M. Rioux, C. K. Erdonmez, S. Hughes, G. A. Somorjai and A. P. Alivisatos, *Science*, 2004, **304**, 711.

30 L. H. Zhang, M. L. Yin, H. P. You, M. Yang, Y. H. Song and Y. J. Huang, *Inorg. Chem.*, 2011, **50**, 10608.

31 G. Tian, Z. J. Gu, X. X. Liu, L. J. Zhou, W. Y. Yin, L. Yan, S. Jin, W. L. Ren, G. M. Xing, S. J. Li and Y. L. Zhao, *J. Phys. Chem. C*, 2011, **115**, 23790.

32 C. C. Huang, T. Y. Liu, C. H. Su, Y. W. Lo, J. H. Chen and C. S. Yeh, *Chem. Mater.*, 2008, **20**, 3840.

33 G. Jia, H. P. You, K. Liu, Y. H. Zheng, N. Guo and H. J. Zhang, *Langmuir*, 2010, **26**, 5122.

34 P. P. Yang, S. L. Gai, Y. C. Liu, W. X. Wang, C. X. Li and J. Lin, *Inorg. Chem.*, 2011, **50**, 2182.

35 F. He, P. P. Yang, D. Wang, C. X. Li, N. Niu, S. L. Gai and M. L. Zhang, *Langmuir*, 2011, **27**, 5616.

36 L. H. Zhang, G. Jia, H. P. You, K. Liu, M. Yang, Y. H. Song, Y. H. Zheng, Y. J. Huang, N. Guo and H. J. Zhang, *Inorg. Chem.*, 2010, **49**, 3305.

37 X. J. Kang, D. M. Yang, P. A. Ma, Y. L. Dai, M. M. Shang, D. L. Geng, Z. Y. Cheng and J. Lin, *Langmuir*, 2013, **29**, 1286.

38 W. Feng, L. D. Sun, Y. W. Zhang and C. H. Yan, *Small*, 2009, **5**, 2057.

39 Z. H. Xu, Y. Cao, C. X. Li, P. A. Ma, X. F. Zhai, S. S. Huang, X. J. Kang, M. M. Shang, D. M. Yang, Y. L. Dai and J. Lin, *J. Mater. Chem.*, 2011, **21**, 3686.

40 R. C. Lv, S. L. Gai, Y. L. Dai, N. Niu, F. He and P. P. Yang, *ACS Appl. Mater. Interfaces*, 2013, **5**, 10806.

41 H. Y. Chen, T. Moore, B. Qi, D. C. Colvin, E. K. Jelen, D. A. Hitchcock, J. He, O. T. Mefford, J. C. Gore, F. Alexis and J. N. Anker, *ACS Nano*, 2013, **7**, 1178.
42 S. B. Yu and A. D. Watson, *Chem. Rev.*, 1999, **99**, 2353.
43 S. J. Zeng, M. K. Tsang, C. F. Chan, K. L. Wong and J. H. Hao, *Biomaterials*, 2012, **33**, 9232.
44 S. J. Zeng, H. B. Wang, W. Lu, Z. G. Yi, L. Rao, H. R. Liu and J. H. Hao, *Biomaterials*, 2014, **35**, 2934.
45 G. Z. Ren, S. J. Zeng and J. H. Hao, *J. Phys. Chem. C*, 2011, **115**, 20141.
46 D. M. Yang, X. J. Kang, P. A. Ma, Y. L. Dai, Z. Y. Hou, Z. Y. Cheng, C. X. Li and J. Lin, *Biomaterials*, 2013, **34**, 1601.
47 J. G. Li, Q. Zhu, X. D. Li, X. D. Sun and Y. Sakka, *Acta Mater.*, 2011, **59**, 3688.
48 Z. Liu, X. M. Sun, N. Nakayama-Ratchford and H. J. Dai, *ACS Nano*, 2007, **1**, 50.
49 Z. Liu, A. C. Fan, K. Rakhra, S. Sherlock, A. Goodwin, X. Y. Chen, Q. W. Yang, D. W. Felsher and H. J. Dai, *Angew. Chem., Int. Ed.*, 2009, **48**, 7668.
50 S. Viswanathan, Z. Kovacs, K. N. Green, S. J. Ratnakar and A. D. Sherry, *Chem. Rev.*, 2010, **110**, 2960.
51 R. D. Shannon, *Acta Cryst.*, 1976, **A32**, 751.
52 C. M. Zhang, C. X. Li, C. Peng, R. T. Chai, S. S. Huang, D. M. Yang, Z. Cheng and J. Lin, *Chem. Eur. J.*, 2010, **16**, 5672.
53 C. X. Li, X. M. Liu, P. P. Yang, C. M. Zhang, H. Z. Lian and J. Lin, *J Phys. Chem. C*, 2008, **112**, 2904.